Journal of Radioanalytical and Nuclear Chemistry (2021) 327:31–37
https://doi.org/10.1007/s10967-020-07504-y

A potential refinement of water endangered with Zn-65 onto modified zeolite

Eva Chmielewská[1] · **Wlodzimierz Tylus**[2]

Received: 30 April 2020 / Accepted: 11 November 2020 / Published online: 4 January 2021

Abstract
The recently synthesized mono- and bimetallic Fe and Mn oxides supported zeolite of clinoptilolite type, characterized with FT-IR, XRD, SEM–EDS and XPS spectroscopy, confirmed the occurrence of a new MnO_2 phase (pyrolusite, birnessite) including mostly amorphous iron oxi(hydr)oxide FeO(OH) species on the surface. The product validated a much higher adsorption capacity toward Zn-65 pollutant compared to the natural clinoptilolite. The following order, beginning with a decreasing maximum adsorption capacity a(max) toward Zn-65 was found: MnOx-zeolite (35.1 mg/g) > FeO(OH)-MnOx-zeolite (23.5 mg/g) > FeO(OH)-zeolite (12.9 mg/g) > natural zeolite (8 mg/g).

Keywords Mn- and Fe-oxides clinoptilolite · XPS · Zn-65 removal · Isotherms

Introduction

In recent years, there has been an increasing use of adsorbents based on natural zeolite (clinoptilolite) supported magnetic nanoparticles or mesoporous oxides with nano-sized pores in the structural framework for environmental remediation and cleanup processes. It is expected that such engineered heterostructures may extend the resultant nanocomposite with entirely new functionalities or superior efficiency in pollutants removal [1, 2].

Various radioactive waste streams are generated by a range of activities including medical and industrial uses through the most significant source, nuclear power generation. The most important nuclides in wastes from reactor operation with respect to clearance are activation products, such as Cr-51, Mn-54, Fe-55, Co-58, Co-60, Ni-63, Zn-65, Sb-125 and fission products, such as Sr-90, Ru-106, Cs-134, Cs-137 and Ce-144. Zn-65 appeared in significant concentrations in early boiling water reactor (BWR) units which employed heat exchangers containing Admiralty (29% Zn) or Muntz metal (40% Zn). In some cases, the condensed secondary steam was contaminated with stable zinc and was used for primary water make-up. The zinc contamination was brought into the primary reactor system where the stable zinc became neutron activated [3].

Zeolites (mainly clinoptilolite) were used for the cleanup of the destroyed nuclear reactor at Chernobyl (former USSR) and for the remediation of the environment after the nuclear accident [4]. Most of the ca. 500,000 tons of zeolite were used for the construction of barriers limiting the spread of radionuclides and for remediation activities such as filtering of drainage waters from the encapsulated reactor, decontamination of the Dnieper River water, and reduction of cesium activity levels in agricultural and veterinary products [5]. Studies showed that a mixture of some natural minerals such as bentonite, mordenite, and clinoptilolite in form of compact layers with thickness of some tens of centimeters may satisfactorily act as buffer materials to protect against radioactive contamination for many years [6]. In this context, natural zeolites are employed as a natural barrier for the migration of radionuclides in the polluted areas around nuclear power station accidents or where nuclear weapons have been stored, such as Chelyabinsk (Russia), Semipalatinsk (Kazakhstan), and Krasnoyarsk (Siberia) [7]. A combination of raw, surfactant-modified, and Ag-impregnated herschelite and a Na-zeolite with chabazite structure was

✉ Eva Chmielewská
chmielewska@fns.uniba.sk

[1] Faculty of Natural Sciences, Comenius University, Ilkovičova 6, Mlynská dolina B2, 842 15 Bratislava, Slovakia

[2] Department of Advanced Material Technologies, Faculty of Chemistry, Wroclaw University of Science and Technology, Wybrzeże Wyspianskiego 27, 50-370 Wroclaw, Poland

also utilized, along with coagulation, sedimentation, and desalination, for the removal of Cs, Sr, Tc, and I from saline radioactive waters after the accident at the Fukushima Daiichi Nuclear Power Plant [8, 9].

A zeolite based permeable barrier (PRB) was also designed in Russia to prevent the further migration of Cs-137 and Sr-90 from the site of the underground nuclear explosion"Kraton-3" performed for peaceful purposes in 1978. Investigations during the period 2007–2008 showed the presence of Cs-137 and H-3 in the water of the region. Zeolitic tuff from Khonguruu (Yakutiya) containing 70–95% HEUtype zeolite (clinoptilolite) was selected for the PRB on the basis of laboratory and modeling studies [7, 10, 11].

Natural zeolite as commonly considered for cation exchanger, is characterized of porous structure and negatively charged framework of AlO_4^{5-} and SiO_4^{4-}—tetrahedras, appropriate to bind or exchange extraframework cations. Based upon the earlier research, Slovakian clinoptilolite is toward Zn(II) not selective, however, chemical modification of its surface allows clinoptilolite to be more effective adsorbent to this metal as well as to be effective even to anionic and aromatic compounds [12].

Experimental

Materials

Natural zeolite of clinoptilolite type originated from the open pit mine at Nižný Hrabovec in the region of east Slovakia neovulcanites and of mordenite type from Bartošova Lehôtka—Paseka in middle Slovakia. While the content of active component in clinoptilolite rock ranges between 70 and 80%, in mordenite rock only about 40% [5, 12]. Over 170,000 metric tonnes of high-grade clinoptilolite were exploited from the open pit mine in Nižný Hrabovec in 2018, making it one of the world's major natural clinoptilolite producer.

A detailed description of FeO(OH)—clinoptilolite sol–gel synthesis is as follows: A 20 g of (0.2–0.8 mm) grain-sized zeolite was mixed with 0.5 L of 10% aqueous solution of iron (III) nitrate nonahydrate [$Fe(NO)_3$•9H2O, Alfa Aesar, crystalline, Germany] and aged at 60 °C in laboratory water bath shaker for 3 days. Then, the 200 mL of 2.5 M KOH solution was added dropwise to prepare the final suspension of pH = 12 and keeping it aged for another 6 days at room temperature. After the reaction period the suspension was filtered and washed with deionized water and finally dried at 105 °C for 2 h in laboratory dryer. The FeO(OH)–MnOx—clinoptilolite was synthesized analogically as FeO(OH)—clinoptilolite, however instead of the natural type, MnOx-clinoptilolite was used as starting material. MnOx-clinoptilolite was prepared by simple and inexpensive large-scale redox-synthesis at ambient temperature using a 5% $KMnO_4$ solution.

Based on the zeolite powdering during the mixing, a sample grain size fraction of 0.2–0.5 mm was selected for the next measurements from originally used 0.2–0.8 mm grain size fraction, using the laboratory sieves (Retsch GmbH, Germany).

Laboratory setup

Experimental batch mode adsorption using 30 mL of the model solution with variable Zn-65 concentration and 0.3 g adsorbents (weight with analytical precision), agitated at constant speed (180 rpm) on a Biosan SIA Multi-Rotator, was carried out for isotherms calculation. To reach equilibrium in the system studied, i.e. Zn(II) aqueous solution versus zeolite based adsorbent, 4 h contact time was necessary. The supernatant solutions were separated through a 0.45 mm cellulose membrane filter and their residual pollutants analysed. All measurements were performed in triplicate. The equilibrium uptake capacity a_{eq} (in mg/g) for each sample was calculated according to the mass balance Eq. (1):

$$a_{\mathrm{eq}} = \left(\frac{C_i - C_{\mathrm{eq}}}{m}\right) V \tag{1}$$

where c (i) and c (eq) were initial and equilibrium concentrations of Zn (II) (in mg/L), m was the mass of adsorbent examined (in g) and V was volume of the solution in liters (L). Chemicls necessary for the stock solution preparation were purchased mostly from Lachema Brno (made in Czech Republic) with analytical grade quality. The stock solution used in the experiments after dilution according to isotherm calculation and plotting (Fig. 3) was prepared from the chemical $Zn(NO_3)_2{\cdot}6H_2O$ in deionized water (pH of 4.8). Radioindicator Zn-65 was supplied by Immunotech Ltd. as $ZnCl_2$ in 0.1 mol HCl (original activity to 18.2.2017: 80 MBq/1.15 cm^3). The radioindicator was the product of Radioisotope Centre Polatom (Poland).

Aqueous model solutions of the metal examined in experiments, labelled with the adequate radioisotope of Zn-65, were determined by means of radioindicator method on spectrometrical set of EG & G Berthold Ortec (USA) with a scintillation detector NaI (Tl).

Analytical equipment

X-ray photoelectron spectroscopy (XPS) studies were carried out using a SPECS PHOIBOS-100 hemispherical spectrometer with a Mg source (1253.6 eV) operating at 250 W for high resolution spectra. The spectrometer energy scale was calibrated using the Au 4f7/2 and Cu 2p 3/2 lines at 84.2 and 932.4 eV, respectively. The powdered samples (with a

diameter under 100 µm) were pressed into a molybdenum sample holder. To better understand the nanomorphology of modified zeolites, grain-sized (0.2–0.5 mm) samples, denoted as coarse, were analysed in the "as received" form or after Ar^+ sputtering. The C1s peak of the carbon at 284.8 eV was used as reference for calculating BEs and counting the number of effects. The spectra were collected and processed by SpecsLab II and CasaXPS v.2.3.19 software.

Scanning Electron Micrograph and elemental SEM–EDS analysis was performed on a JEOL JSM 6390LV Electron Microscope JEOL JFC-1200. Table 1 represents the average weight percentage of the elements in individual sample calculated from 5 to 10 measurements depending on sample´s homogeneity.

The X-ray powder diffraction (XRPD) analyses were carried out using a Philips diffractometer PW1710 with the generator PW1870 and the vertical goniometer PW3020,

equipped with a secondary graphite monochromator. Measurements were performed in the following regime: radiation source: CuKα radiation was used with the applied voltage of 40.00 kV and 20.00 mA current, scanning range: 2 = 4°–70°, step size: 0.02°, exposition time: 0.80 s/step. The resulted patterns were compared with the JCPDS Cataloque (Joint Commettee on Powder Diffraction Standards No. 22-1236, 13-0304 for clinoptilolite verification).

Results and discussion

SEM–EDS and SEM

The XRD measurements did not reveal any clinoptilolite matrix destruction or enrichment with a new Fe crystalline phase. All recorded diffractometer traces were typical for well crystallized clinoptilolite, corresponding with d spacings. It is assumed that the new embedded FeO(OH) hydrogels into the mesoporous structure of zeolitic rock (natural and MnOx-clinoptilolite) in the form of the amorphous phase with a content below 10 wt% might result in an indetectable change of both X-ray diffractograms [13]. Only the visible peaks of the primary deposited manganese dioxide (MnO_2), like pyrolusite onto the surface of natural zeolite or the MnOx-zeolite was determined, where the Mn wt% content in some of the darkest surface spots reached even 38 wt% according to SEM–EDS.

Table 1 displays an average weight percentage of the elements, acquired by SEM–EDS from 10 measured various spots of individual samples. While the results obtained by SEM–EDS in wt% represent a surface profile of nanocomposites studied approximately up to 50 nm deep, the results provided by XPS method are in at% and mean analyses up to 5 nm under the outer surface. In general, when comparing both analytical techniques, an inhomogeneous coating and dispersion of Fe(III) and Mn(IV) metallic species on the zeolitic surface was noted. Coarse nanocomposites, grain-sized in 0.2–0.5 fraction, acquired a colour between black and dark red, which were original colours of individual MnOx- and FeO(OH)-zeolites. The SEM photomicrograph of FeO(OH)-MnOx-zeolite (Fig. 1) clearly shows typical clinoptilolite´s sheets, well-defined and tabular shaped crystals with small external covering (right in the lower corner) of agglomarated needle-like and flake-like inclusions. Needle-like inclusions may resemble the morphology of akaganeite and pyrolusite, being flake-like to lepidocrocite.

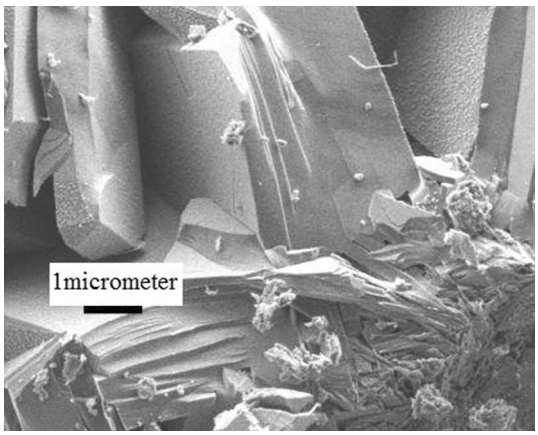

Fig. 1 A surface morphology under SEM of prepared FeO(OH)-MnOx- zeolite of clinoptilolite type

Table 1 An average SEM–EDS composition of natural zeolite of clinoptilolite type and its 3 modified samples

Element wt% ± Error	Natural zeolite	FeO(OH)-zeolite	MnOx-zeolite	FeO(OH)-MnOx-zeolite
Oxygen	52.19 ± 1.02	55.19 ± 2.02	53.62 ± 0.86	57.43 ± 3.37
Magnesium	0.42 ± 0.05	0.45 ± 0.13	0.09 ± 0.15	0.51 ± 0.13
Aluminum	5.16 ± 0.15	4.34 ± 0.27	2.11 ± 0.19	4.26 ± 0.33
Silicon	27.32 ± 0.65	20.97 ± 0.83	20.06 ± 0.28	25.17 ± 1.57
Potassium	2.05 ± 0.09	3.67 ± 0.25	0.89 ± 0.16	5.14 ± 0.39
Calcium	1.13 ± 0.08	5.36 ± 0.98	9.15 ± 0.34	5.04 ± 0.26
Manganese	–	0.09 ± 0.31	8.42 ± 0.80	1.11 ± 0.26
Iron	1.01 ± 0.1	3.75 ± 1.01	0.84 ± 0.52	4.48 ± 0.47

X-ray photoelectron spectroscopy

X-ray Photoelectron Spectroscopy (XPS), as a surface-sensitive quantitative spectroscopic technique, was used to measure the elemental composition and chemical state of the elements that characterized the surface of recently prepared nanocomposites.

According to XPS measurements, the surface content of Ca(II) ions in the clinoptilolite was about 1.2 at% with the binding energy (BE) of $Ca2p_{3/2}$ at 348.65 eV (Fig. 2a). After immobilization of iron oxides onto zeolite, only a trace amount of Ca(II) ions remained in the outer surface. A part of calcium (5.5 at%) was, as it can be seen, supplied externally when zeolite was treated with $KMnO_4$ solution. Interestingly enough, its quantity on the surface became 5 times higher than the content of total manganese. That calcium content remained on the adsorbent grains also in the FeO(OH)-MnOx-modified zeolite, despite that the manganese content decreased. It is supposed, that the 5% of Ca(II) presents completely new substance, with BE of 347.32 eV, what is characteristic for $CaCO_3$.

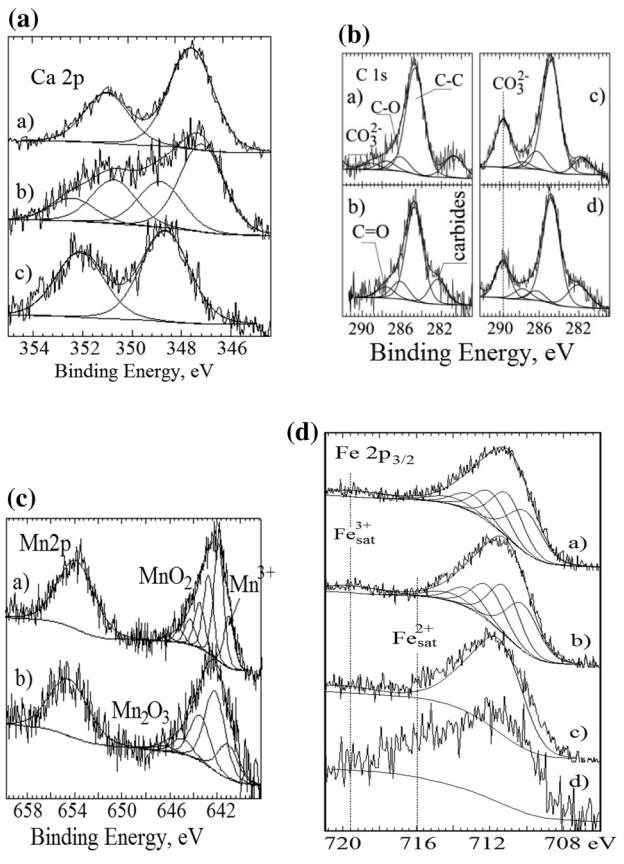

Fig. 2 **a** The Ca 2p core level spectra of MnOx-zeolite surface (**a**), MnOx-zeolite powdered and **b** natural zeolite (**c**); **2b** XPS C 1 s core level spectra of natural zeolite surface (**a**), FeO(OH)-zeolite (**b**), MnOx-zeolite (**c**) FeO(OH)-MnOx-zeolite; **2c** Mn2p core level spectra of (**a**) MnOx-zeolite and **b** FeO(OH)–MnOx-zeolite; **2d** Fe $2p_{3/2}$ core level spectra of (**a**) FeO(OH)-zeolite, **b** FeO(OH)-MnOx-zeolite, **c** FeO(OH)-zeolite powdered and **d** natural zeolite

A typical or native Ca(II) ion of clinoptilolite may be observed on the surface of MnOx-powdered zeolite (Fig. 2a, b). Differences in the calcium content of MnOx– zeolite coarse and powdered, illustrate the surface sensitivity of XPS method very well. On the outer surface of coarse MnOx-zeolite, only $CaCO_3$ was identified. Thus, the analysis of powdered MnOx-zeolite validates "bulk" composition, i.e. in addition to the covering with $CaCO_3$, exchangeable Ca(II) ions were explored as well. Some carbonate groups (at ca. 290 eV) on the surface of both coarse MnOx-zeolite and FeO(OH)-MnOx-zeolite as $CaCO_3$ were observed, respectively.

Using the alkalic precipitation, more exchangeable Ca cations may become replaced with Fe(III) cations, however, Mn(IV) cations might not participate in the cation exchange process, which is likely due to lower selectivity of clinoptilolite toward Mn(IV) cations. Based on deconvolution of the Mn2p envelope of MnOx-zeolite, it may be concluded that the only form of manganese compound was MnO_2 (Fig. 2c). The small peak at the lower BE region of spectrum shows Mn(III) valency, which does not correspond to the MnO_2 multiplet. It was estimated to 15% of the total amount of manganese content. This share is considered to be characteristic for pyrolusite (regarding to ca. 10% in the pure MnO_2 powder) [14].

Immobilization of FeO(OH) onto MnOx-zeolite caused a significant decrease of Mn content, from 1.04 to 0.37 at% and simultaneously its reduction, probably to Mn_2O_3, which corresponds to the parameters displayed. The Mn2p core level spectra of MnOx– zeolite show at BE 654 eV and of FeO(OH)-MnOx-zeolite at BE 655 eV potential $KMnO_4$ peak (Fig. 2c), which is probably left from the treatment of samples with $KMnO_4$ solution [14, 15]. An attempt for detailed analysis of Fe oxidation states was performed on the basis of Fe $2p_3/2$ high resolution spectra and their chemical shifts.

For quantitative speciation assignment of the multiplet envelope and other structures to each chemical state is necessary. However, in regard to the transition metals, the fitting of complex multiple species for iron is quite difficult. The work represents the research results that were compared with the results published in [14, 15]. All spectral fitting parameters for Fe 2p3/2, such as binding energy (eV), percentage of the total area (%), FWHM value (eV) as relative ratios as well as spectral component separation (eV) originate from above authors.

However, in order to achieve the best fitting, proportionally higher FWHM values were applied (as a consequence of low Fe content in the samples, the higher pass energy had to be taken). For both the coarse FeO(OH)-zeolite and FeO(OH)-MnOx-zeolite, as well as according to deconvolution recorded

in Fig. 2d–a and d–b, a pronounced fitting was observed, when only FeOOH species are assumed to be present. The peak shape of powdered FeO(OH)-MnOx-zeolite (Fig. 2d–c) was a little different and thus impossible to deconvolute. It can be seen that the intensity of Fe 2p3/2 photoelectrons was slightly higher in the area of 715–716 eV. Such energy is characteristic for Fe(II) satellite peak. It is very likely that it comes from the bulk of the sample and belongs to the composition of clinoptilolite.

To confirm this prediction, a spectrum of pure clinoptilolite was added (Fig. 2d–c). It seems that in a clinoptilolite the iron does not form a homogenous phase (mixture of Fe(III) and Fe(II)) and thus deconvolution may be not reliable. After immobilization of FeO(OH) onto MnOx-zeolite, a significant decrease of manganese content was observed. Moreover, surface oxidation with KMnO4 solution was less invasive on the clinoptilolite structure than the alkalic FeO(OH) precipitation, in which the structure Al(III) ions may undergo some partial replacement with Fe(III) ions.

This fact corresponds well with the Si/Al ratio arising from the value of 4.2 for natural zeolite to 4.5 for MnOx-zeolite, to 5.3 for FeO(OH)-MnOx-zeolite and to 6.2 for FeO(OH)-zeolite. Indeed, when analyzing the zeolite quantitative results and adequate ratios between the actual metals of coarse FeO(OH)-MnOx-zeolite (Mn/Fe = 0.18, Fe/Al = 0.57 and Fe/Si = 0.11) and powdered FeO(OH)-MnOx- zeolite (Fe/Al and Fe/Si were lower − 0.29 and 0.06, but the ratio Mn/Fe = 0.18 was exactly the same), it may be concluded that manganese was not covered with iron, since this ratio (Mn/Fe) should also be smaller. It is assumed that Mn(IV) occured as MnO_2, was in deep profiles of zeolitic structure as crystalline or chemically bound.

Zn(II) adsorption

Table 2 and Fig. 3 present the adsorption results on various surface-modified zeolite samples including the natural one using the statistical least square method (MW XP, Microsoft Office Excel 2007, Regression Analysis). The equilibrium data from Fig. 3 were analysed by two parameter empirical adsorption isotherm models Langmuir (2), Freundlich (3) and BET (4) as well as with three parameter Redlich-Peterson isotherm (5) which fit the parameters listed in Table 2.

$$\frac{1}{a} = \left(\frac{1}{a_{\max} \cdot b \cdot c(\mathrm{eq})}\right) + \left(\frac{1}{a_{\max}}\right) \tag{2}$$

$$a = K \cdot c(\mathrm{eq})^{\frac{1}{n}} \text{ or } \log a = \log K + \frac{1}{n} \log c(\mathrm{eq}) \tag{3}$$

$$\frac{c(\mathrm{eq})}{a\left(c_{\mathrm{sat}} - c_{\mathrm{eq}}\right)} = \frac{1}{K_{\mathrm{BET}} \cdot a_{\max}} + \frac{K_{\mathrm{BET}} - 1}{K_{\mathrm{BET}} \cdot a_{\max}} \cdot \frac{c(\mathrm{eq})}{c(\mathrm{sat})} \tag{4}$$

Table 2 Langmuir, Freundlich, BET and Redlich-Peterson isotherms data for Zn(II) adsorption onto natural, FeO(OH)–, FeO(OH)–MnOx– and MnOx-zeolite of clinoptilolite type

Adsorbent/		Langmuir isotherm			Freundlich isotherm		BET isotherm			Redlich-Peterson isotherm		
Zn(II)	a (max) mg/g	K_L L/mg	R^2	n	K_F L/mg	R^2	K_{BET}	R^2	g	A L/g	B (L/mg)^g	R^2
Natural zeolite/Zn(II)	8.02	0.162	0.9548	8.5106	3.567	0.9524	−5.937	0.9510	0.9400	2.756	0.176	0.9988
FeO(OH)–zeolite/Zn(II)	12.87	0.053	0.9974	2.9095	1.682	0.7875	−5.311	0.9632	1.0003	2.784	0.081	0.9973
FeO(OH)-MnOx-zeolite/Zn(II)	23.50	0.048	0.9998	6.2775	8.535	0.9832	0.985	0.9851	1.1466	2.783	0.018	0.9958
MnOx-zeolite/Zn(II)	35.10	0.056	0.9996	2.1882	2.671	0.9563	0.991	0.9769	1.2421	2.831	6.448	0.9986

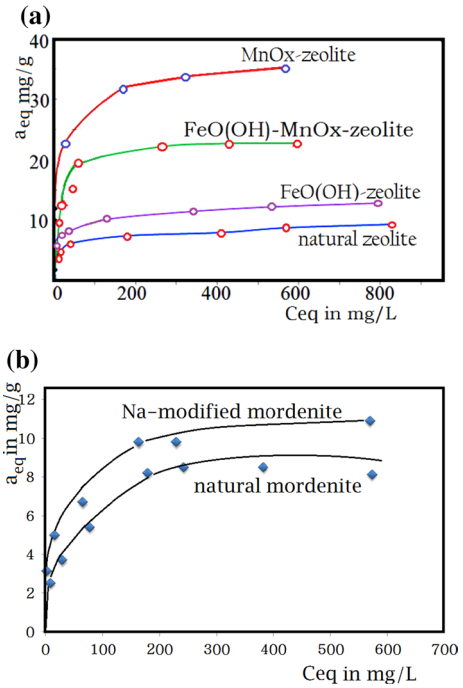

Fig. 3 Experimental adsorption isotherms for Zn(II) in aqueous solution versus zeolite of clinoptilolite type and zeolite modified with manganese polyoxides or iron oxihydroxides (**a**) and ditto versus Na modified zeolite of mordenite type (upper curve) and natural mordenite (lower curve) (**b**)

$$a = \frac{A \cdot c(\mathrm{eq})}{1 + B \cdot c^{g}(\mathrm{eq})} \quad \text{or} \quad \ln\left(A\frac{C_{\mathrm{eq}}}{a} - 1\right) = g\ln\left(C_{\mathrm{eq}}\right) + \ln(B) \tag{5}$$

where a means the specific adsorption capacity, a(max) the maximum adsorption capacity in mg/g, c(eq) the equilibrium concentration in solution in mg/L, b relates to the affinity of the solute for the binding sites expressed in L/mg, $c$sat or co means saturation concentration in solution in mg/L and A, B and g are non linear regression constants of Redlich-Peterson isotherm.

As can be seen from R^2 (determination coefficient) values, the Langmuir model gives a slightly better description of Zn(II) adsorption onto all the samples studied than the Freundlich and BET and Redlich-Peterson models of isotherm, but not for the system of natural zeolite/Zn(II), which fitted better to Redlich-Peterson isotherm (Table 2). The Langmuir isotherm is used to describe sorption on highly homogenous surfaces smoothly, but is not quite adequate for adsorption on surfaces with a lot of irregularities. On the other hand, the Freundlich isotherm contains the heterogeneity factor (n), which relates to the affinity of adsorbing surface, and thus partially compensates for these irregularities. In other words, the Freundlich equation is a special case for heterogeneous surface energies, in which the energy term varies as a function of surface coverage.

According to Fig. 3 and Table 2 the following order with a decreasing maximum adsorption capacity a(max) toward Zn(II) was found: MnOx-zeolite (35.1 mg/g) > FeO(OH)-MnOx-zeolite (23.5 mg/g) > FeO(OH)-zeolite (12.9 mg/g) > natural zeolite (8 mg/g). With regard to natural zeolite of clinoptilolite type, because MnOx-zeolite reached 4-times higher capacity toward Zn(II), coated manganese polyoxides on the external and partially internal zeolite surface may work as parallel adsorbent. Zn(II) ions from solutions may also intercalate mechanically between parallel layers, which is typical for some manganese oxide structure (birnessite), and likely occurs on the zeolite surface as well (Fig. 3, Table 2). More effective adsorption of FeO(OH)- and FeO(OH)-MnOx-zeolites toward Zn-65 might be related with presence of various finaly dispersed Fe(III) hydrogels as well, which bind this pollutant through complexation reactions.

In Fig. 3b, there are plotted also experimental adsorption isotherms for Zn(II) in aqueous solution measured with the Na ions pretreated mordenite in regard to the natural mordenite, however the maximum adsorption capacities toward Zn(II) recorded were low (8.14 mg/g and 8.52 mg/g), more or less comparable only with the natural clinoptilolte.

As aforementioned, the novel FeO(OH)-MnOx binary oxides coated clinoptilolite with abundant surface hydroxyl groups, synthesized by a simultaneous oxidation and co-precipitation method and combining the oxidation property of manganese polyoxides and the adsorption and affinity features of iron oxihydroxides, presents some kind of upgraded clinoptilolite, which may be used for more effective water remediation applications than the natural clinoptilolite.

Conclusions

Iron and manganese oxides supported, bimetallic zeolite of clinoptilolite type, which due to nanoporous structure of zeolitic carrier worked as nanoreactor and in such a treated form provided enhanced functionalities, were prepared and thoroughly investigated. The recently synthesized nanocomposites validated much higher adsorption capacity toward Zn(II) pollutant than the natural clinoptilolite. The Zn(II) removal efficiency of domestic monoionic Na-modified mordenite was comparable only with the removal efficiency of the natural clinoptilolite. Such a decontamination procedure may be considered for perspective and advantageous, based on natural resources, which are economic feasible and globally accessible products.

Acknowledgements XPS analyses were financed by a statutory grant allocation from the Polish Ministry of Science and Higher Education

to the Faculty of Chemistry of Wrocław University of Science and Technology. The authors express a great thank for the support.

References

1. Li Y, Huijuan L, Chunlei L, Huachun L, Jiuhui Q (2016) Magnetically-confined Fe-Mn bimetallic oxide encapsulation as an efficient and recoverable adsorbent for arsenic (III) removal. Particle Particle Syst Charact 33:323–331
2. Krauklis A, Ozola R, Burlakovs J, Rugele K, Kirillov K, Trubaca-Boginska A, Rubenis K, Stepanova V, Klavins M (2017) FeOOH and $Mn_8O_{10}Cl_3$ modified zeolites for As(V) removal in aqueous medium. J Chem Technol Biotechnol 92:1948–1960
3. Kazemian H (2012) Environmental applications of natural zeolites, Chap. 10. In: Inglezakis VJ, Zorpas AA (eds) Handbook of Natural Zeolites, Bentham-e-Books, pp 214–237
4. Pansini M (1996) Natural zeolites as cation-exchangers for environmental protection. Miner Deposita 31:563–575
5. Chmielewská E (2014) Environmental zeolites and aqueous media: examples of practical solutions. Betham Science Publishers, Sharjah
6. Galamboš M, Paučová V, Kufčáková V, Rosskopfová O, Rajec P, Adamcová R (2010) Cesium sorption on bentonites and montmorillonite K10. J Radioanal Nucl Chem 284:55–64
7. Chelishchev NF, Volodin VF, Krjukov VL (1988) Ionoobmennye svoistva prirodnych vysokokremnistych ceolitov. Nauka, Moskva
8. Yamagishi I, Nagaishi R, Kato C, Morita K, Terada A, Kamiji Y (2014) Characterization and storage of radioactive zeolite waste. J Nucl Sci Technol 517–518:1044–1053
9. Misaelides P (2019) Clay minerals and zeolites for radioactive waste immobilization and containment: a concise overview, Chap. 10. In: Mercurio M, Sarkar B, Langella A (eds) Modified clay and zeolite nanocomposite materials, environmental and pharmaceutical applications. Elsevier, Amsterdam, pp 243–265
10. Seneca SM (2012) Evaluation of a natural zeolite permeable treatment wall in the removal of strontium-90 from groundwater: installation to long-term performance, Ph.D. thesis. Department of Civil, Structural and Environmental Engineering S.U.N.Y. Buffalo NY.https://pqdtopen.proquest.com/doc/1030445743.html?FMT5AI
11. Misaelides P, Sarri S, Kantiranis N, Noli F, Filippidis A, de Blochouse B (2018) Investigation of chabazitic materials as Cs-137 sorbents from cementitious aqueous solutions. Micropor Mesopor Mater 266:183–188
12. Chmielewská E, Lesný J (2012) Selective ion exchange onto Slovakian natural zeolites in aqueous solutions. J Radioanal Nucl Chem 293:535–543
13. Chmielewská E, Tylus W, Drábik M, Majzlan J, Kravčak J, Williams C, Čaplovičová M, Čaplovič Ľ (2017) Structure investigation of nano-FeO(OH) modified clinoptilolite tuff for antimony removal. Micropor Mesopor Mater 248:222–233
14. Biesinger MC, Payne BP, Grosvenor AP, Lau LWM, Gerson AR, Smart RSC (2011) Resolving surface chemical states in XPS analysis of first row transition metals, oxides and hydroxides: Cr, Mn, Fe, Co and Ni. Appl Surface Sci 257:2717–2730
15. Laszczyńska A, Tylus W, Szczygieł B, Szczygieł I (2018) Influence of post—deposition heat treatment on the properties of electrodeposited Ni–Mo alloy coatings. Appl Surface Sci 462:432–444